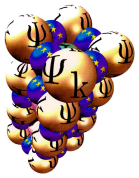

Ψ_k Scientific Highlight Of The Month

No. 125 **October 2014**

Theory of solid/electrolyte interfaces

Axel Groß[1]

Institut für Theoretische Chemie, Universität Ulm, Albert-Einstein-Allee 11, 89069 Ulm, Germany.

[1] axel.gross@uni-ulm.de

Theory of solid/electrolyte interfaces*

Axel Groß

Institut für Theoretische Chemie, Universität Ulm,

Albert-Einstein-Allee 11, 89069 Ulm/Germany

Email: axel.gross@uni-ulm.de

* This is a shortened version of a book chapter that will appear in *Surface and Interface Science, Vol. 7: Solid/Liquid and Biological Interfaces* . Edited by Klaus Wandelt.

I. INTRODUCTION

Processes at solid/electrolyte interfaces have witnessed an increasing interest in recent years. This is caused by the importance of the electrochemical energy storage and conversion which will play a central role in our future energy technology [2]. Among the devices in which such processes occur are batteries, fuel cells, and electrolysers. However, solid/electrolyte interfaces have in fact been a research subject for a very long time. The first concepts describing solid/electrolyte interfaces were based on macroscopic approaches in which the electrolyte was described as a dielectric medium. Currently, there is a trend towards an electrochemical surface science approach [3] trying to identify structures and processes at solid/electrolyte interfaces with an atomic resolution.

Still, in spite of the relevance of processes occuring at solid/electrolyte interfaces, it is fair to say that our knowledge about the atomistic structure is rather limited. Experimentally, this is due to the fact that the number of experimental probes with atomic resolution at the solid-liquid interface is still limited compared to the solid-vacuum interface. In particular techniques based on the scattering and diffraction of electronic beams do not work in solution. solid/electrolyte interfaces includes a proper description of the liquid which requires to determine free energies instead of just total energies. Furthermore, in electrochemistry, structures and properties of the electrode-electrolyte interfaces are governed by the electrode potential. These two facts add considerable complexity to the theoretical description [4]. Consequently, even such elementary properties as the exact structure of water at electrode-electrolyte interfaces are still debated [5]. This lack of knowledge is illustrated in Fig. 1.

Figure 1a shows a typical schematic drawing of the structure of solid/electrolyte interfaces that can be found in textbooks. A figure like this is used to illustrate the differences between anions and cations at interfaces. Cations typically adsorb *non-specifically*, i.e. their solvation shell stays intact upon adsorption on the electrode. In contrast, anions often bind *specifically* to the electrode with their solvation shell being broken up. Yet, in such drawings assumption of the arrangements of the water molecules are made which are often depicted as balls with an arrow denoting the dipole moment of the water molecule. Panel a suggests that all water molecules might bind to the electrode in the same configuration. On the other hand, panel b shows the optimized structure of a water layer on a Pt(111) electrode covered by fluorine atoms at a coverage of 1/12 determined by density functional theory (DFT) calculations. Although the water layer is wrapped around the fluorine atoms, it is obvious that due to the

Surface and Interface Science, Vol. 7: Solid/Liquid and Biological Interfaces . Edited by Klaus Wandelt.

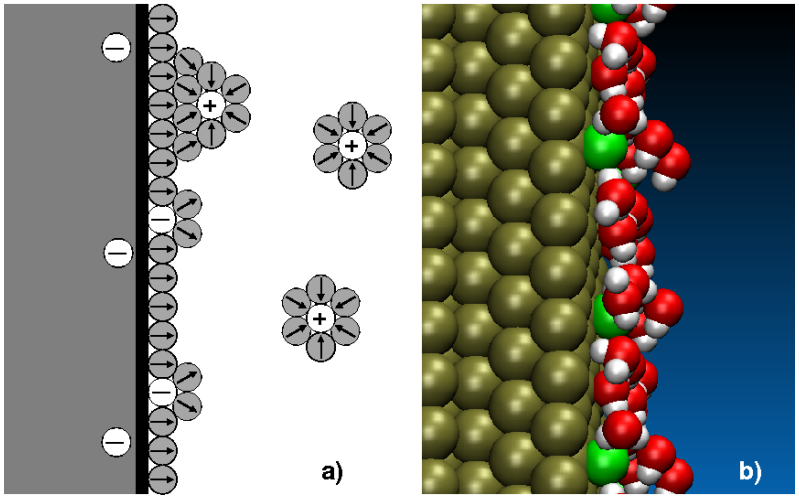

FIG. 1. Interface between a metal electrode and an aqueous electrolyte. a) Schematic drawing, b) Optimized structure of a water layer on a halide-covered Pt(111) electrode obtained by density functional theory calculations (courtesy of Florian Gossenberger).

strong hydrogen bonding between the water molecules there is still a water network present in which the water molecules assume different orientations. Furthermore, note that thermal disorder is not considered neither in panel a nor in b.

This example shows that nowadays first-principles electronic structure calculations can be rather helpful in gaining information about the structure of solid/electrolyte interfaces. Although, as mentioned above, some obstacles still have to be overcome, significant progress in the theoretical description of solid/electrolyte interfaces has been made recently, as will be shown in this chapter. Still it is fair to say that our understanding of solid/electrolyte interfaces is incomplete.

In this chapter, first a simple, but elegant model to take the electrochemical environment within a thermodynamical approach into account is described. In a second step, continuum models of solid/electrolyte interfaces will be discussed. The atomistic description of solid/water interfaces will then be addressed, and current approaches to incorporate varying electrode potentials into the theoretical description will be covered. Non-aqueous electrolytes will be briefly discussed, and finally an outlook for future work will be given. It will become obvious that the theory of solid/electrolyte interfaces is far from being complete in spite of the numerous theoretical studies on this subject. Because of this large number, an exhaustive and comprehensive review of important studies in this field is not possible.This chapter rather presents selective examples in order to illustrate our current understanding. We hope

Surface and Interface Science, Vol. 7: Solid/Liquid and Biological Interfaces . Edited by Klaus Wandelt.

that it might encourage further studies about this subject which is not only scientifically very interesting but also technologically rather relevant.

II. STRUCTURE OF ELECTROCHEMICAL INTERFACES

Processes at electrochemical electrodes occur in the presence of the electrolyte under potential control. As described above, this makes their theoretical description rather challenging. Electrolytes typically contain a certain amount of ions which serve as the charge carriers of the ionic transport. Due to the intimate contact of the electrode with the electrolyte, the presence of the ions in the electrolyte will lead to a certain coverage of them on the electrode which is a function of the thermodynamic variables such as electrode potential or the concentration of the electrolyte. Here we will describe how the ion surface coverage can be estimated from DFT calculations and basic thermodynamic considerations. We will first address the case of gas/solid interfaces whose treatment is less complex due to the absence of varying electrode potentials.

In heterogeneous catalysis, processes occur at such solid-gas interfaces. Note that the impingment rate of the gas-phase particles is often so low, even at ambient conditions, that the presence of the gas does not have to be explicitly considered in the theoretical modeling but implicitly through the corresponding chemical potential of species present in the gas phase. In equilibrium, the Gibbs free energy of adsorption $\Delta\gamma$ for $N_{\rm ads}$ adsorbates bound to a surface area A_s at a given temperature T and pressure p can be expressed [6] as

$$\begin{aligned}\Delta\gamma(T,p) &= \gamma(T,p,N_{\rm ads}) - \gamma_{\rm clean}(T,p,0) &(1)\\ &= \frac{1}{A_s}\Delta G^{ads}(T,p) &(2)\\ &= \frac{N_{\rm ads}}{A_s}\left(E_{\rm ads} - \Delta\mu_{\rm ads}(T,p)\right)\ . &(3)\end{aligned}$$

Here, $\Delta G^{ads}(T,p)$ is the change in the free energy upon adsorption. In the last line of eq. (3), $E_{\rm ads}$ is the total adsorption energy per particle as obtained from DFT calculations, i.e., in the limit of zero temperature and pressure. $\Delta\mu_{\rm ads}(T,p)$ is the temperature and pressure dependent part of the chemical potential of the adsorbate. Any change in entropy and zero-point energies upon adsorption can be taken into account, but in fact it is often neglected in theoretical studies addressing systems in heterogeneous catalysis and surface science as these contributions are typically small [6].

In the adsorption at electrochemical interfaces, the reference state does not correspond

to the atom or molecule in gas phase – whose energy is relatively easy to determine – but rather to the species in solution in the presence of an electrode potential U. This means that the chemical potential μ has to be replaced by the electrochemical potential

$$\tilde{\mu} = \mu + neU\,, \tag{4}$$

where n is the charge of the particle. Still the problem remains that the electrochemical potential includes all solvation effects of the species. The determination of solvation energies requires computationally demanding thermal integration schemes [7]. These efforts can be avoided using the concept of the computational hydrogen electrode [8, 9]. It is based on the fact that at standard conditions (pH= 0, $p = 1\,\mathrm{bar}$, $T = 298\,\mathrm{K}$) $U = 0$ is defined as the electrode potential at which there is an equilibrium between a proton and an electron in aqueous solution $\mathrm{H^+(aq)} + e^-$ and hydrogen in the gas phase, $\frac{1}{2}\mathrm{H_2(g)}$. Furthermore, it is well known how the electrochemical potential of the proton and the electron change if the proton concentration and the electrode potential is varied [10], namely according to

$$\tilde{\mu}(\mathrm{H^+(aq)}) + \mu(e^-) = \frac{1}{2}\mu(\mathrm{H_2(g)}) - eU_{\mathrm{SHE}} - k_{\mathrm{B}}T\ln(10)\mathrm{pH}\,, \tag{5}$$

where U_{SHE} is the electrode potential with respect to the standard hydrogen electrode (SHE). The success of the computational hydrogen electrode is among others based on the fact that it allows to derive adsorption energies with respect to solvated species without the need to determine any solvation energies.

This concept does not only work for hydrogen and protons, it works also for any redox couple $\frac{1}{2}\ \mathrm{A_2} + e^- \rightleftarrows \mathrm{A^-}$ [11]. The electrochemical potential is then given by

$$\tilde{\mu}(\mathrm{A^-(aq)}) - \mu(e^-) = \frac{1}{2}\mu(\mathrm{A_2(g)}) + e(U_{\mathrm{SHE}} - U^0) + k_{\mathrm{B}}T\ln a_{\mathrm{A^-}}\ , \tag{6}$$

where U^0 is the reduction potential of the corresponding halide and $a_{\mathrm{A^-}}$ its activity coefficient. Neglecting the change of zero-point energies and the entropy change upon adsorption, one arrives at the following expression for the free energy of adsorption as a function of the electrode potential at standard conditions, i.e. for an activity $a_{\mathrm{A^-}} = 1$,

$$\Delta\gamma(U_{\mathrm{SHE}}) = \frac{N_{\mathrm{ads}}}{A_s}\left(E_{\mathrm{ads}} - e(U_{\mathrm{SHE}} - U^0)\right)\ . \tag{7}$$

For other concentrations of species A in the electrolyte, the corresponding electrode potential has to be shifted by $k_{\mathrm{B}}T\ln a_{\mathrm{A^-}}$ which corresponds at room temperature to about 60 meV when the activity is changed by one order to magnitude. Within this approach, the

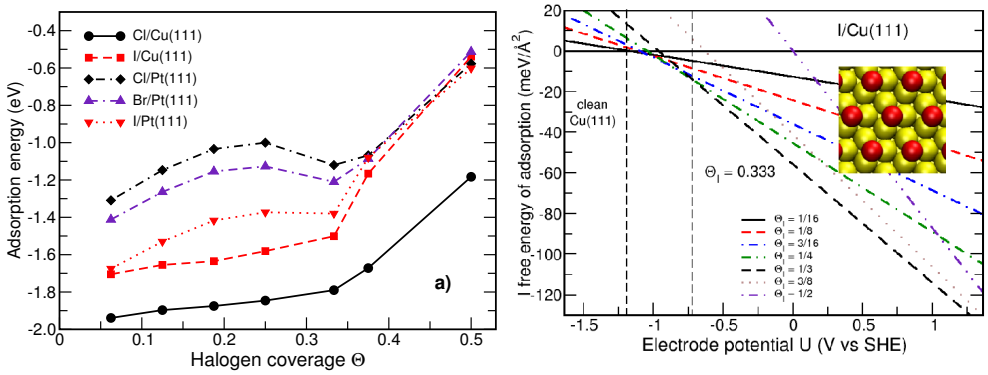

FIG. 2. Adsorption of halides on metal surfaces. a) Adsorption energies of halogen atoms on Cu(111) and Pt(111) with respect to the free halogen molecule as a function of the coverage [13]; b) calculated electrochemical equilibrium coverage of iodine on Cu(111) at standard condition as a function of the electrode potential vs. SHE. The inset illustrates the structure of the iodine $\sqrt{3} \times \sqrt{3}$ structure (after [14]) .

adsorption energy E_{ads} appearing in Eq. 7 is calculated without taking the electrochemical environment into account. Furthermore, the varying excess charge at the metal electrodes as a function of the electrode potential is also not considered. Still this approach has been successfully used to derive electrochemical trends in the oxygen reduction [8, 12] and in the hydrogen evolution [9] which belong to the most important reactions in electrocatalysis.

Here we will illustrate this approach with respect to the equilibrium coverage of halides on metal electrodes [14]. In Fig. 2a, the adsorption energies of various halides on Cu(111) and Pt(111) as a function of the coverage with respect to the corresponding halogen molecules in the gas phase are plotted. Typically, adsorbed halides show a repulsive interaction due to the dipole-dipole interaction. Interestingly enough, the $\sqrt{3} \times \sqrt{3}$ structure corresponding to a coverage of 1/3 is rather stable, especially for chlorine and bromine on Pt(111). Note that the close-packed $\sqrt{3} \times \sqrt{3}$ structure is at the same time the structure with the largest *and* smallest mutual distances among the adsorbates for a given density. This might explain its stability for adsorbates that repel each other.

Still, from the adsorption energies alone it is not directly evident what the thermodynamically stable structures under specific conditions are. In Fig. 2b, the free energy of adsorption of iodine on Cu(111) determined according to Eq. 7 is plotted as a example. Indeed it is found that at potentials above -0.7 V, only the $(\sqrt{3} \times \sqrt{3})$ structure is stable. This is consistent with the experiment [15]. For the sake of completeness it should be mentioned that at

positive potentials close to the onset of the copper dissolution a uniaxially incommensurate iodide adlayers caused by a unidirectional compression of the $\sqrt{3} \times \sqrt{3}$-I structure has been observed [16], which, however, is hard to model in periodic DFT calculations.

III. CONTINUUM MODELS OF SOLID/ELECTROLYTE INTERFACES

The interface between a solid and a electrolyte typically corresponds to an interface between an electron conductor (the electrode) and an ionic conductor (the electrolyte) [10]. Usually such interfaces are charged: there is an excess charge at the surface of the electrode which is compensated by a charge layer of opposite sign at the solution side of the interface. This charge distribution acts as a capacitor with a small effective plate separation and is therefore called the *electric double layer*. The earliest model of the electric double layer is usually attributed to Helmholtz who assumed that the charge distribution in the solution is realized as a single layer of ions is adsorbed at the surface [21]. The potential of this fixed *Helmholtz layer* exhibits a linear behavior.

This model was refined early in the 20th century by Gouy [22] and Chapman [23]. They allowed for a diffuse thermal distribution of the ions. Applying Boltzmann statistics for the distribution of both anions and cations of absolute charge $|ze|$ with a bulk density of n_0, one arrives at the *Poisson-Boltzmann equation* [10] for the potential $\phi(x)$

$$\frac{d^2\phi}{dx^2} = -\frac{zen_0}{\varepsilon\varepsilon_0}\left(\exp\left(-\frac{ze\phi(x)}{k_BT}\right) - \exp\left(\frac{ze\phi(x)}{k_BT}\right)\right) \tag{8}$$

For $ze\phi(x)/k_BT \ll 1$, the exponentials can be linearized so that the solution of the Poisson-Boltzmann equation yields an exponentially decreasing electric potential

$$\phi(x) = \frac{\sigma}{\varepsilon\varepsilon_0\kappa}\exp\left(-\kappa z\right) \ , \tag{9}$$

where σ is the surface charge density of the electrode and

$$\kappa = \left(\frac{2(ze)^2 n_0}{\varepsilon\varepsilon_0 k_BT}\right)^{1/2} \ , \tag{10}$$

is the inverse *Debye length*. Such a formulation is in fact close to the macroscopic treatment of semiconductor interfaces incorporating space charge layers.The Gouy-Chapman model, however, does not take into account that some ions adsorb specifically at the electrode surface, i.e., they are not mobile. Therefore it fails for highly charged double layers. For example, the Gouy-Chapman model predicts that the capacity as a function of the potential

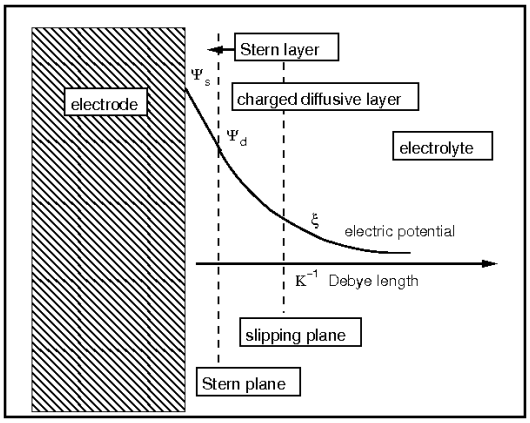

FIG. 3. Illustration of the Stern model.

always has its minimum at the potential of zero charge, but at higher concentrations of the electrolyte a much more complex dependence of the capacity on the potential is found [10].

In order to improve the description of the double layer, a combination of the Helmholtz and Gouy-Chapman models was suggested by Stern [24]. This model is illustrated in Fig. 3, giving an internal Stern layer (i.e. Helmholtz layer) in which the potential drops linearly, and an outer diffuse layer (i.e. Gouy-Chapman layer) in which the potential drops exponentially. The capacity C of this arrangement is then given

$$\frac{1}{C} = \frac{1}{C_{\mathrm{GC}}} + \frac{1}{C_{\mathrm{H}}} \tag{11}$$

where C_{GC} is the Gouy-Chapman capacity and C_{H} is the Helmholtz capacity that is independent of the electrolyte concentration.

This model yields a phenomenological description of the solid/liquid interface. It is very helpful in order to understand and analyze general trends of the capacity at electrochemical interfaces. Still as a continuum model it does not take the atomistic structure of the interface into account. Hence a more quantitative theory of solid/electrolyte interfaces is needed.

IV. ATOMISTIC FIRST-PRICINPLES DESCRIPTION OF SOLID/WATER INTERFACES

In order to get a more realistic picture of the structure of solid/electrolyte interfaces, an atomistic modeling of solid/electrolyte interfaces is necessary. In order to describe the electrolyte, the solid electrode and the solid-electrolyte interaction properly, a first-principles

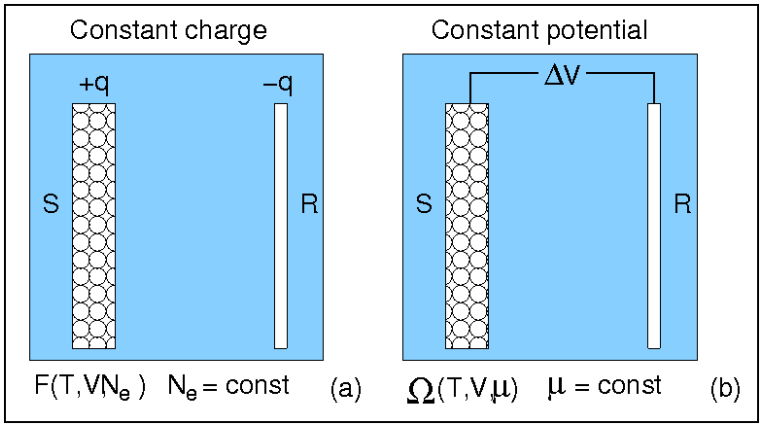

FIG. 4. Illustration of a) the constant charge ($N_e = const$) and b) the constant chemical potential ($\mu = const$) mode to treat charged systems within periodic DFT calculations. The corresponding thermodynamical potentials to describe a slab together with a reference electrode are the Helmholtz free energy F and the grand potential Ω, respectively.

treatment is usually necessary. The full version of this section can be found in [1], the reader might also have a look at Refs. [49, 91].

V. EXPLICIT CONSIDERATION OF VARYING ELECTRODE POTENTIALS

In section II, we have shown how varying electrode potentials can be implicitly included in the expression for the corresponding electrochemical potentials. However, the explicit influence of varying electrode potentials on, e.g., adsorption energies can thus not been assessed. Note that varying electrode potentials lead to changes in the excess surface charge of the electrodes and the emergence of electric fields. Dealing with charged systems in periodic electronic structure calculations is not trivial as the unit cell has to stay charge-neutral. Hence the excess charge has to be balanced by counter charges.

There are in fact two different modes to deal with charged systems in periodic DFT setups [102] that are illustrated in Fig. 4. Originally, DFT was formulated for systems with a constant number of electrons N_e, but then it was realized [103] that there is an equivalent grand canonical formulation of DFT in which the chemical potential μ of the electrons

instead of the number of electrons is one of the basic quantities.

Systems with a constant number of electrons correspond to a slab that is isolated from its environment. In order to obey charge neutrality, a counter electrode carrying charge of equal amount as the slab but opposite sign has to be placed within the unit cell. This can be realized in different fashions, for example as a capacitor, as shown in Fig. 4a, but the compensating charge does not need to be locally separated from the charged slab. It can also be distributed uniformly over the unit cell as a compensating charge background [104]. This is in fact the default procedure in periodic DFT codes. They automatically include a homogeneous compensating charge background when the system is charged due to the fact that in the Ewald summation typically done in reciprocal space the monopole term is excluded since it leads to divergence.

The "μ = constant" mode, on the other hand, corresponds to a metallic slab that is part of an electric circuit in which the voltage between charged electrode and counter electrode is specified. This mode is in fact much closer to an electrochemical setup in which the electrode potential is a crucial input parameter. There are implementations of periodic DFT calculations that perform self-consistent iterations within the grand-canonical formulation of DFT [102, 105]. The electron density is calculated in each iteration step as a sum of partial densities over Kohn-Sham orbitals with eigenvalues up to a given chemical potential μ. As a consequence, the number of electrons is not necessarily conserved.

However, this mode is not as easy to implement into periodic DFT codes as the "N_e = constant" mode. Furthermore, it typically exhibits a much slower convergence of the self-consistent field cycles than calculations with a fixed number of electrons. Hence the vast majority of first-principles studies addressing electrochemical systems so far have been performed at a constant number of electrons.

Still, also calculations in the "N_e = constant" mode can be related to the "μ = constant" mode in an *a posteriori* fashion. First calculations are performed for a given number of electrons. Then the corresponding electrode potential is specified. In general, any different configuration calculated for a given number of electrons corresponds to a different electrode potential as dipole moments and consequently the work function vary. In practice, constant charge calculations are performed for a number of different charge states, the corresponding electrode potentials are determined, and then the desired quantity is interpolated as a function of the electrode potential so that it can be obtained for a given arbitrary potential. This will be demonstrated below using the oxygen dissociation [106] as an example.

We will now address specific approaches to realize constant charge calculations and derive

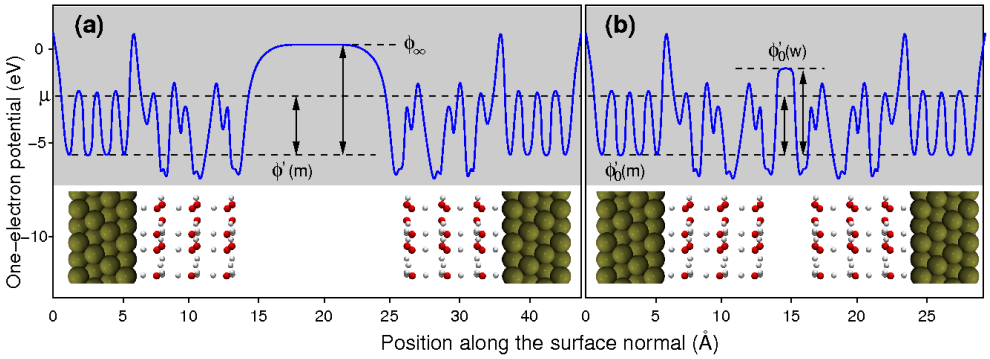

FIG. 5. Electrostatic energy profile across the unit cell for solvated water slabs in a periodic slab calculation with (a) and without (b) a vacuum region in the middle between the metal slabs. μ_e denotes the chemical potential of the electrons which corresponds to the Fermi energy at $T = 0\,\mathrm{K}$. ϕ_∞ is the vacuum level and $\phi'(\mathrm{m})$ and $\phi'_0(\mathrm{m})$ are the bulk metal potential with and without the presence of the vacuum layer in the calculations, respectively (after [104]).

the corresponding electrode potentials. As already mentioned above, the default procedure in periodic DFT codes to treat charged systems is charge compensation through a homogeneous background. Two problems arise in such an approach. First, the compensating charge background interacts with all charges present in the supercell. This artificial interactions has to be corrected for. Second, in the presence of a compensating charge background there is no vacuum region in the unit cell. Hence neither the work function can be directly calculated and nor the electrode potential be derived.

These two problems were addressed in the so-called "double-reference method" [104, 107] which is illustrated in Fig. 5. In a first step, a DFT calculation with a well-defined vacuum region is performed. This is achieved by constructing a solvated slab with a vacuum region introduced in the middle of the unit cell between the slabs, as illustrated in Fig. 5a. The potential in the middle of the vacuum layer is used as the first reference by setting $\phi_\infty = 0$. Then it is assumed that the electrode potential does not change when the vacuum layer in the water region is omitted as depicted in Fig. 5b.

In regions deep in the interior, the potential variation does not depend on the presence of the vacuum region. Note also that electric fields do not penetrate into perfect metallic conductors but are shielded at the surface though the build-up of a surface charge. Hence the potential $\phi_0(m) = \phi'_0(m) - \phi_\infty$ inside of the slab taken with respect to the vacuum level is taken as the first reference point, where the primed values indicate the unshifted values and the subscript 0 denotes the uncharged calculations without a vacuum.

For a charged slab, however, the presence of the excess charge q leads to the existence of an additional electric field at the interface and in the region between the metallic slabs. Since there is then no longer any region where the one-electron potential is flat, a vacuum reference point can not be established. The following procedure has been suggested within the "double-reference method" [107]: A region far from the electrode is fixed at its configuration in the $q = 0$ calculation, and the one-electron potential $\phi_0(w)$ at this site (see Fig. 5b) is used as the second reference point. The remaining system is relaxed under the influence of the applied charge, and the potential at all other positions is shifted with respect to the second reference point. Finally, to obtain an absolute electrode, for example versus the normal hydrogen electrode, the work function for the H_2/H+ couple on Pt in standard conditions is substracted. In the definition of the electrode potential one has to take into account that in electrochemistry potentials are typically defined with respect to a positive probe charge whereas work functions and one-electron potentials are defined for a negative probe charge.

Naively one could think that the introduction of a constant charge background does not affect the variation of the one-electron potential as no electric field might be associated with a homogeneous charge that is translationally invariant. However, one has consider that the constant charge background is embedded in the varying charge density of the water-metal system, and the resulting electrostatic potential as a solution of the Poisson equation is a consequence of the whole charge distribution subject to the appropriate boundary conditions. Even in vacuum regions where the charge distribution is entirely given by uniform background charge, this introduces an electric field caused by a varying potential as the general solution of the Poisson equation for a region with a constant charge background

$$\nabla^2\phi(\mathbf{x}) \;=\; 4\pi\rho_o \;. \tag{12}$$

in Cartesian coordinates is given by

$$\phi(\mathbf{x}) \;=\; 4\pi\rho_o \left(\sum_{i,j=1}^{3} C_{i,j} x_i x_j + \sum_i C_i x_i + C_0 \right) \tag{13}$$

with $\sum C_{ii} = 1$.

Note first that for an infinitely extended isolated uniform charge background, i.e. without any compensating charges, there is no proper solution of Eq. (12). This reflects the fact that the electrostatic energy density diverges for such a system. In the case of a finite region of constant charge density, however, the potential follows a quadratic profile according to

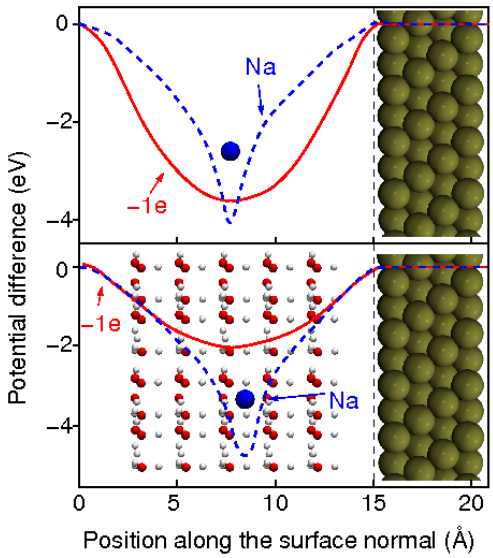

FIG. 6. Calculated potential difference $\Delta\phi$ between a charged and uncharged Cu(111) slabs with the excess electron density compensated either by a constant charge background (denoted by $-1e$) or by a Na ion pseudopotential without (upper panel) and with a water layer (lower panel) in front of the electrode (after [104]. Note that the plotted atoms are only included as an illustration and do not correspond to the actual positions of the atoms in the calculations.

Eq. (13). This is illustrated in Fig. 6 where in the upper panel the calculated potential difference $\Delta\phi$ [104] between a charged and uncharged Cu(111) slab with the excess charge compensated by a constant charge background as a function of the vertical position (indicated by $-1e$) is plotted. This variation can be understood if one takes into account that for positions displaced from the centre of the vacuum region there are unequal amounts of charge in both directions along the surface normal.

One may also explicitly include counter ions at the approximate position of the outer Helmholtz plane as a model for the electrochemical interface instead of balancing the excess charge of the slab by a constant charge background. The corresponding potential difference with a sodium ion pseudopotential as the counter ion is also plotted in Fig. 6. This leads to the same formal surface charge density as the compensating charge background. Yet, the resulting potentials are quite different for the two methods. Already close to the metal slab the slope of the two potential curves differs significantly. In the case of the constant charge background, an electric field results that is more than a factor of two larger close to the electrode. This illustrates that a uniform compensating charge background and an explicit counter charge lead in general to rather different potentials. Similar problems arise in the

modelling of charged vacancies in semiconductors.

The upper panel of Fig. 6, however, does not correspond to an electrochemical situation as the electrolyte is not properly taken into account. In the lower panel of Fig. 6 the same counter charge distributions are considered as in the upper panel, but in an aqueous environment [104]. Now the difference is considerably reduced, apparently because of screening effects of the polarizable water layers. In particular across the inner water layer directly above the metal electrode, the resulting electric fields are now rather similar. This indicates that the continuum technique might be appropriate to model electrochemical processes occuring in the inner layer as long as the electrolyte is represented through a polarizable medium. Still one has to be cautious that the introduction of a constant charge background can introduce artefacts in the description of electrochemical interfaces.

There is a further problem arising in the modelling of counter charges. As a positive counter charge is attracting electrons, it lowers the potential for the electrons. If this lowering is large enough so that the work function of the metal is smaller than the depth of the potential minimum due to the counter charge, then there will be an artificial charge flow from the metal slab to the counter charge. This always needs to be checked when performing slab calculations with a positive compensating charge background.

The artefacts associated with a uniform compensating charge background can be avoided if the counter electrode is explicitly considered. This can be done by representing the counter electrode as a localized planar charge distribution [81, 108–112], for example in the form of a Gaussian profile perpendicular to the surface:

$$\rho_{ce}(\mathbf{r}) = \frac{q}{\sqrt{2\pi}\alpha} \exp\left(-\frac{z - z_0}{2\alpha}\right)^2 , \tag{14}$$

where q is the total charge of the counter electrode and z_0 corresponds to the position of the counter electrode. The width of the Gaussian charge distribution α should be chosen for the sake of numerically convenience [81].

This particular approach is illustrated in Fig. 7. The extra electronic charges on the electrodes are compensated by the planar Gaussian-shaped counter electrode. Figure 7 also shows some examples of laterally averaged one-electron potentials for different excess electron numbers per unit cell for a symmetric slab covered by one water-layer. The varying electron number leads to a shift of the Fermi energy whose range is indicated $\Delta\varepsilon_{\mathrm{F}}$.

Note that for negatively charge slab the counter electrode has to be positively charged which makes it attractive for electrons. However, for a sufficiently large positive counter charge the one-electron potential in the counter electrode drops below the Fermi energy

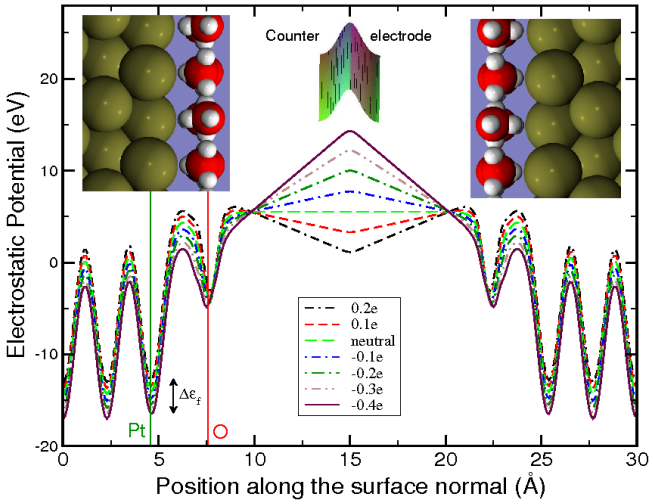

FIG. 7. Illustration of the implementation of explicit Gaussian-shaped counter electrode in periodic DFT setup together with laterally averaged one-electron potential of a symmetrically constructed metal-water slab for varying electron numbers given per unit cell (after [81]).

defined by the number of electrons in the slabs. This would lead to an artifial electron transfer from the slabs to the counter electrode, as mentioned above. Hence the range towards negative charges on the slabs corresponding to low electrode potentials is limited.

The electric field strength in the vacuum region caused by the counter electrode can be deduced from the slope of the linear regions. It does not penetrate deep into the Pt electrode since it is screened by the metallic properties of the Pt(111) slab. Hence inside of the slab the averaged one-electron potential is just shifted in a parallel fashion.

The counter charge has been introduced in order to compensate the excess charges on the electrodes, otherwise it has no physical relevance. Still there is a direct electrostatic interaction between the electrons and the ion core with the counter electrode, in spite of the fact that the counter electrode and the considered atoms are separated in space.

Therefore, the resulting total energy has to be corrected for this interaction which can be done, as derived by Taylor *et al.* [104], by integrating the electrochemical potential μ over the applied charge, i.e.,

$$E = \int_0^q \mu dQ \;=\; E_{\rm DFT} + \int_0^q \left[\int \frac{V_{\rm tot}}{\Omega} d^3x \right] dQ \;. \tag{15}$$

A further correction is required to take the varying number of electrons in each system into account. Thus the total grand canonical free energy energy of the electrons, except for

entropic effects is given by

$$E_{\text{free}} = E + \mu q \, . \tag{16}$$

Here E is the total energy from the DFT calculations corrected for the electrostatic interaction with the counter electrode as given by Eq. 15, and q is the total charge of the electron-ion system. The electrochemical potential μ has been taken with respect to the reference system with $q = 0$.

It is obvious from Fig. 7 that for non-zero excess charge there is no field-free region in this implementation, similarly to the case with a compensating uniform charge background. Hence also here no vacuum level can be straightforwardly defined which also means that no work function and hence no electrode potential [113] can be directly deduced. One way to determine the electrode potential in this method is to relate the charge to the potential via experimentally derived capacities [109], however, this introduces an empirical component to this approach.

In principle, a similar first-principles approach as in the double reference method [104] describe above could be used to specify the electrode potential. However, as Fig. 7 illustrates, there is a very convenient second reference point as requested by the double reference method. All the one-electron potentials drawn in Fig. 7 cross outside the water layer at a position z_{ref} where the electrode potential in the neutral case already assumes its vacuum level. Using z_{ref} as a second reference point, simply the difference between the potential at this reference point and the Fermi energy can be regarded as a measure of the work function

$$\Phi = v\left(z_{ref}\right) - \varepsilon_F \tag{17}$$

The corresponding electrode potential U of the water-covered metal electrode relative to the normal hydrogen electrode can then be estimated [104, 113, 114] by

$$U = \Phi - \Phi_{\text{NHE}} \, . \tag{18}$$

where the value of Φ_{NHE} can be taken from the literature. There is still some debate about the exact value of Φ_{NHE}, often $\Phi_{\text{NHE}} = 4.44\,\text{V}$ [115] is assumed.

This approach has been used to address the Volmer reaction

$$\text{H}_3\text{O}^+ + e^- \leftrightarrow \text{H}_{\text{ad}} + \text{H}_2\text{O} \tag{19}$$

on Pt(111) by calculating the energy of a Pt(111) substrate covered with one ice-like bilayer in a $2\sqrt{3} \times 2\sqrt{3}$ geometry with one hydrogen atom per unit cell either adsorbed on the electrode or incorporated into the water bilayer leading to H_3O^+.

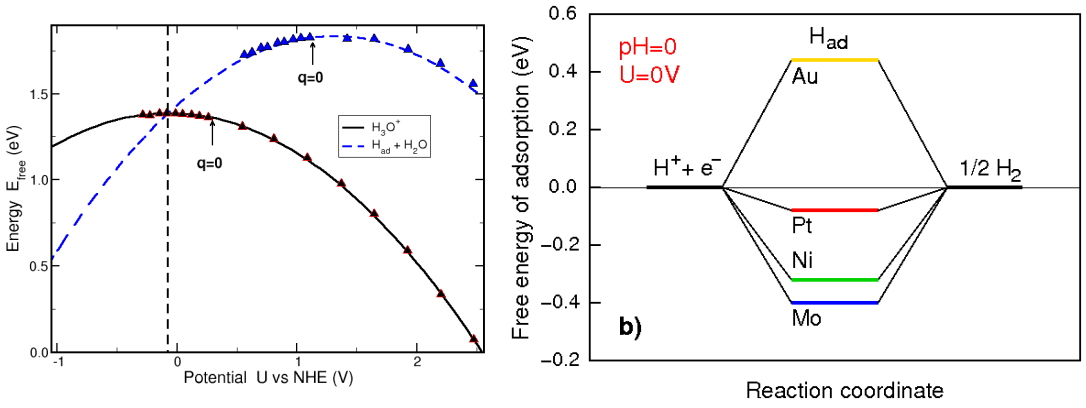

FIG. 8. a) Free energy calculated according to eq. (16) as a function of the electrode potential vs NHE for a water bilayer on Pt(111) with an adsorbed hydrogen atom (H_{ad} + H_2O) and with a solvated proton in the water bilayer (H_3O^+) in a $2\sqrt{3} \times 2\sqrt{3}$ geometry, calculated using the explicit counter electrode according to Eq. 14. The symbols correspond to the calculated values, the line to a quadratic fit to these results (after [81]); b) Free energy diagram for hydrogen evolution at equilibrium (U=0 vs NHE) derived from hydrogen adsorption energies at various metal electrodes (adapted from Ref. [9]).

The free energies of both structures as a function of the electrode potential vs NHE are plotted in Fig. 8a. The difference $E_{\text{free}}(H_{ad} + H_2O)$ - $E_{\text{free}}(H_3O^+)$ between these two curves can be regarded as an estimate for the adsorption energy of the hydrogen atom with respect to a proton in solution. The equilibrium of the Volmer reaction is at about -0.08 V vs NHE, which means that it is rather close to the equilibrium of the hydrogen evolution at standard conditions. As a consequence, the hydrogen evolution on Pt(111) with the intermediate adsorbed hydrogen state is essentially thermo-neutral which has in fact been realized as the reason why Pt is an excellent catalyst for the hydrogen evolution [9].

This conclusion is illustrated in Fig. 8b where the calculated hydrogen adsorption energies on Au, Pt, Ni and Mo using the concept of the computational hydrogen electrode [9] according to Eq. 5 are plotted. For the hydrogen evolution reaction (HER), as for any catalytic reaction, the Sabatier principle is valid: the interaction between the catalyst and the substrate should be neither too strong nor too weak. For a very weak interaction, the reactant will not bind to the catalyst and no reaction will occur. For a rather strong interaction, the reactant and/or the reaction products are not able to desorb from the catalyst again. This concept is the basis for the volcano plots in heterogeneous and electro-catalysis [116, 117].

Hence an intermediate interaction strength between reactant and catalyst is optimal for

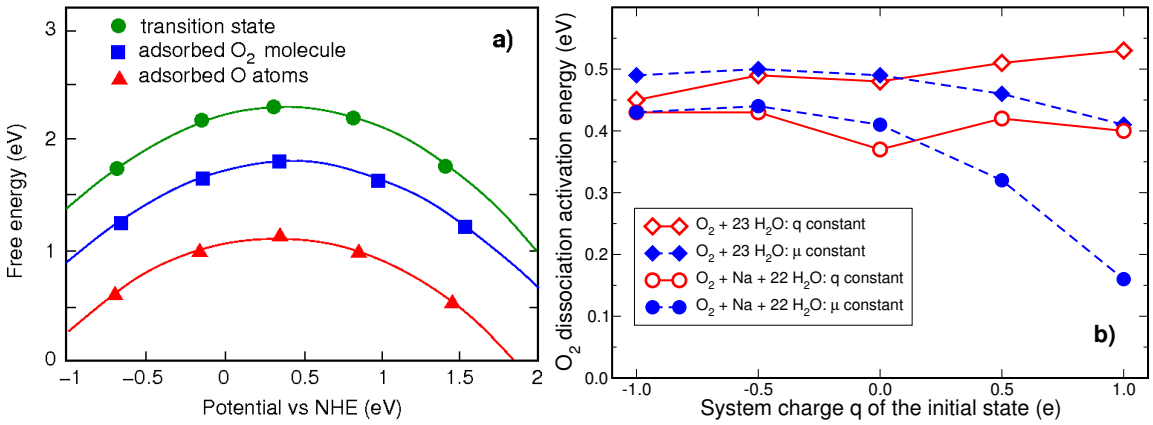

FIG. 9. a) Calculated Free energies as a function of potential for the initial, transition and final state of O_2 dissociation on solvated Pt(111) obtained with the double reference method [104]. The symbols correspond to the results obtained for different charge states of the Pt electrode whereas the solid curves are quadratic fits to the results. b) Dissociation barrier of O_2 on solvated Pt(111) without and with Na coadsorption, respectively, for various constant system charges q of the system and for constant potential, kept at the corresponding value of the initial state (adapted from Ref. [106]).

any catalytic reaction. As Fig. 8b shows, Pt indeed exhibits this intermediate interaction with hydrogen, where Au binds hydrogen too weakly and Ni and Mo too strongly. The free energies calculated as a function of the electrode potential in Fig. 8a fully confirm the exceptional role of Pt for the HER illustrated in Fig. 8b. It should still be noted that for the determination of the free energies in Fig. 8 the Pt(111) electrode has been assumed to be clean whereas at low potentials Pt(111) electrodes should be water-covered. The consideration of coverage effects might lead to some quantitative modifications, but probably not to any qualitative changes.

As a further application of a constant charge scheme we will present the oxygen dissociation on Pt(111) [106] which has been addressed using the double reference method [104]. The initial, transition and final state of the O_2 dissociation on Pt(111) in the explicit presence of water molecules without and with Na coadsorption has been calculated for various system charges, and the corresponding potential has been derived. Figure 9a shows the free energies as a function of potential for the case without the Na atom. In order to derive the activation barrier for O_2 dissociation for a specific potential, the difference between the interpolated quadratic fits is taken. These barriers in the "μ = constant" mode are plotted

in Fig. 9b where the charge of the initial state is used as a reference.

However, Fig. 9b also illustrates the difference between the constant charge and constant potential mode, as also the activation barrier at constant charge is plotted. In particular for positively charged Pt(111), i.e. at positive electrode potentials, there is a large difference between the results in these two modes, the corresponding activation barriers differ by up to 0.2 eV. This deviation can be traced back to the difference in the respective electrode potentials between the initial and the transition state in Fig. 9b (boxes and circles, respectively) at positive charge. If the states for a given charge are aligned above each other, as in the case of negative potential or charge, then there is only a small difference between the constant charge and the constant potential mode. Basically this means that the involved states are associated with rather similar work functions. If, however, the states are not aligned, as in the case of positive charges, then significant differences can result. This also means that AIMD simulations in the constant charge mode might give unreliable results as barriers can be severely under- or over-estimated. The differences between the constant charge and the constant potentiak mode in fact decrease with increasing size of the surface unit cell. If the studied reaction involves only a small fraction of the considered atoms, then the associated work function change will only be small, even if locally the dipole moment changes.

Up to here we have presented two ways to realize compensating charges in a constant charge mode for periodic DFT calculations, through a uniform charge background and through an explict Gaussian-shaped counter electrode. Note that there are also other possibilities to implement a explicit counter charge into a periodic DFT arrangement, for example through a perfect conducting continuum with a non-vanishing surface charge above the slab in a two-dimensional periodic approach [118–121]. This so-called effective screening method has among others been used to address the structure of water under acidic conditions [119, 120, 122].

All these constant-charge methods use excess charges in order to model varying electrode potentials. However, in an electrochemical cell changing the electrode potential is accompanied by a rearrangement of the counter ions in the electrolyte which supply in fact the charges at the electrode/electrolyte interface. Hence in fact no charged unit cells are needed but just the concentration of counter ions at the electrode surface has to be varied to reach another electrode potential. This idea has been employed by Nørskov, Rossmeisl and coworkers [114, 123] in a periodic DFT setup. They have changed the corresponding electrode potential by introducing hydrogen atoms in the water layer close to the metal electrode. The added hydrogen atoms either become solvated as protons leading to the formation of hydro-

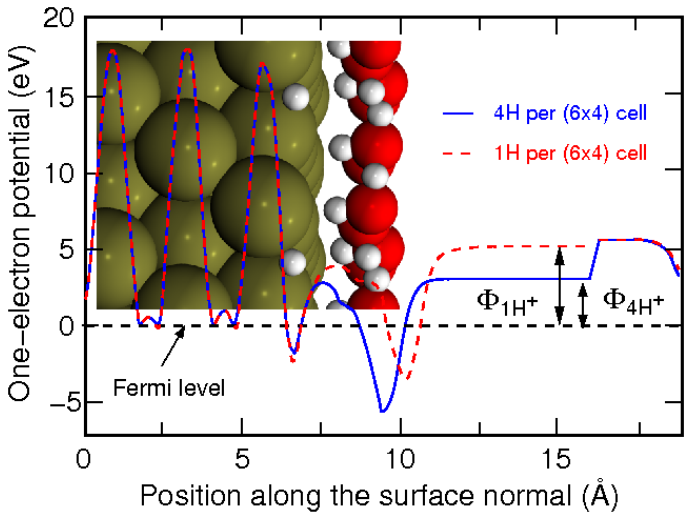

FIG. 10. Illustration how the work function and thus the electrode potential is changed by varying the number of counter ions at the electrode/electrolyte interface. The one-electron potential is changed by varying the number of hydrogen atoms in the water layer at Pt(111) within a (6×4) geometry. In the vacuum layer, there is a potential drop due to the presence of a dipole layer (adapted from Ref. [114]). The inset illustrates the structure of the interface with additional protons.

nium ions (H_3O^+) or adsorb at the metal electrode. In either case they change the work function of the electrode/electrolyte system and thus the corresponding electrode potential.

This elegant method is illustrated in Fig. 10. In this setup, the whole supercell always remains neutral so that no countercharges are needed. By changing the hydrogen concentration, the surface charge and hence the electrode potential can then be varied. In Fig. 10, the laterally averaged one-electron potential is shown for two different concentrations of hydrogen atoms, one or four atoms per (6×4) supercell. The particular atomic configuration is illustrated in the inset.

It can be clearly seen that the two different hydrogen concentrations lead to vastly different work functions which are given by the difference between the flat potential in the vacuum region and the Fermi level. The corresponding electrode potential, for example versus the normal hydrogen electrode, can be derived using eq. 18.

This approach has also been used to address the hydrogen evolution reaction on Pt(111) [114]. The potential was varied by adding varying amounts of hydrogen atoms to supercells of different size. In detail, the elementary processes occuring in the hydrogen evolution reaction

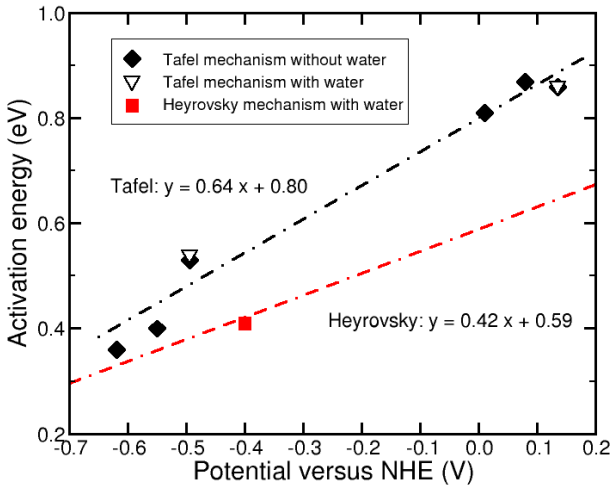

FIG. 11. Calculated activation energy for the Tafel reaction as a function of potential without (diamonds) and with (triangles) a water bilayer and for the Heyrovsky reaction with water (circles). For the Heyrovsky reaction, two further barriers were determined which lie outside the plotted potential range. The dashed lines correspond to linear fits to the data (adapted from [114]) .

on Pt(111), namely the Volmer reaction

$$\mathrm{H}^+ + e^- \rightarrow \mathrm{H}_{\mathrm{ad}}\,, \tag{20}$$

the Tafel reaction

$$2\mathrm{H}_{\mathrm{ad}} \rightarrow \mathrm{H}_2\,, \tag{21}$$

and the Heyrovsky reaction

$$\mathrm{H}_{\mathrm{ad}} + \mathrm{H}^+ + e^- \rightarrow \mathrm{H}_2\,. \tag{22}$$

were addressed using this approach. In spite of its importance in electrochemistry, there is still some debate about the exact mechanism of the hydrogen evolution reaction [124, 125].

The barriers for the three reactions given above were calculated for a set of given hydrogen concentration. This ansatz faces the same problem as constant charge simulations, the configurations along the reaction path correspond to different dipole moments and thus electrode potentials. Therefore, as representative of the potential at which the reaction occurs the average of the initial and final state potentials was taken. Note that the uncertainty associated with this procedure decreases with the size of the unit cell.

The calculated activation barriers as a function of the potential for the Tafel reaction at the electrode-vacuum interface and in the presence of a water bilayer and for the Heyrovsky

reaction in a water bilayer are plotted in Fig. 11. Additionally calculated data points for the Heyrovsky reaction lie outside of the plotted potential range. There is a large gap between the results for negative and for positive potentials. This is due to the fact that there is a discontinuity in the differential hydrogen adsorption energies once a complete hydrogen layer is formed. The gap in Fig. 11 could only be closed if larger unit cells were chosen or if some extrapolation scheme [123] is employed.

As Fig. 11 indicates, the dependence of the barriers on the potential is approximately linear. The so-called transfer coefficient α

$$\alpha = \frac{dE_a}{d\phi}\,, \tag{23}$$

is given by the slope of the linear fit to the data. It is regarded as a measure of the symmetry of the activation barrier. The value of $\alpha = 0.64$ for the Tafel reaction indicates that the barrier location for the Tafel reaction is closer to the initial state at the electrode, whereas $\alpha = 0.42$ for the Heyrovsky mechanism means that in this case the barrier is located closer to the outer Helmholtz plane.

At potentials around 0 V, the Pt electrode becomes covered by a monolayer of hydrogen. Further hydrogen adsorption only occurs at potentials below -0.5 V which corresponds to the so-called opd hydrogen (over-potential deposited). Whereas the activation barriers are rather large at positive potentials, both the Tafel and the Heyrovsky reaction exhibit moderate barriers at negative potentials where hydrogen evolution becomes thermodynamically possible. As Fig. 11 shows, the calculated barriers for the Heyrovsky mechanism are smaller than for the Tafel mechanism. This suggests that the Heyrovsky reaction should dominate the hydrogen evolution. Experimentally, the mechanism for the hydrogen evolution on Pt electrodes has been found to depend on the electrode termination [124]. As far as Pt(111) is concerned, the exact reaction mechanism could not be unambiguously deduced, the measured activation energy of 0.18 eV [124], however, is smaller than the one calculated in the DFT study [114]. Thus there is still room for further improvements in the theoretical description.

So far we have only discussed calculations performed within the constant charge mode, as this mode is much easier to implement as the constant potential mode. In the constant potential mode, the number of electrons has to be allowed to vary. Thus a grand-canonical formulation of DFT has to be invoked in which the chemical potential μ of the electrons instead of the number of electrons N is one of the basic quantities [103]. The theoretical framework for such a constant potential approach has been discussed by Lozovoi *et al.* [102].

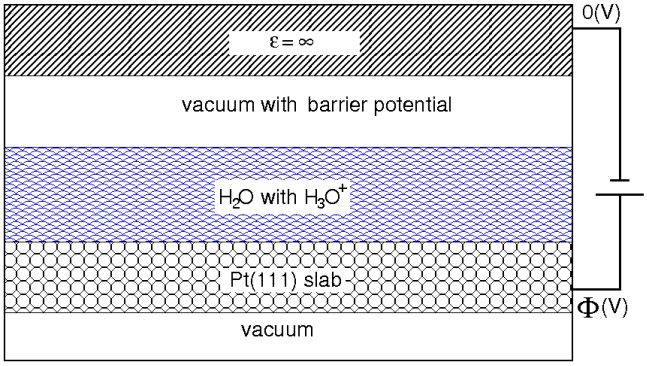

FIG. 12. Computational setup to perform constant potential calculations within the effective screening method [126]

They have proposed a method in which the number of electrons is allowed to vary in the self-consistent field procedure such that the Fermi level stays at a preset value. However, as it turns out, such an approach can lead to instabilities in the practical implementation [126] caused by oscillations in the number of electrons [127].

In order to avoid these problems Bonnet *et al.* [126] implemented a scheme in which the system described within the effective screening method mentioned above is connected to a fictitious potentiostat. The setup is illustrated in Fig. 12. In this particular implementation [118, 119], the system is described periodically in two dimensions, but not in the dimension perpendicular to the electrode. In detail, the laterally periodic slab that can be covered by water and/or adsorbates is placed between two polarizable continua characterized by their dielelectric constant ϵ. For electrochemical systems, vacuum ($\epsilon = 1$) can be chosen at the metal side and a perfect conductor ($\epsilon = \infty$) at the other side.

The potentiostat operates analogously to a thermostat. In the Nosé-Hoover thermostat [128], the temperature is controlled by allowing the exchange of kinetic energy with an external thermostat at temperature T. Analogously, in this constant potential scheme, the system is allowed to exchange electronic charge with an external potentiostat at a specified potential so that the total electronic charge of the system becomes a dynamical variable. Dynamical equations for the total electronic charge are used such that the calculated trajectory samples the grand-canonical distribution at a given electrode potential.

Recently another constant potential scheme was proposed for DFT calculations in a non-periodic finite setup [127]. This avoids the introduction of compensating counter charges. Still, a straightforward implementation of a grand-canonical DFT scheme by inserting the requested chemical potential μ of the electrons into the Fermi-Dirac distribution functions

leads also in a finite set-up to numerical instabilities. Instead, a numerical evaluation of $d\mu/dN$ is employed in order to arrive at a good guess for the correct number of electrons N.

Both of these presented constant potential implementations have not been routinely applied in the description of structures and processes at the electrochemical solid/electrolyte interface. Hence their robustness and reliability still has to assessed. It is in general true that still several different approaches have been suggested to model varying electrode potentials, and there is no consensus yet about what is the most appropriate method. This is an indication that the first-principles description of electrochemical electrode-electrolyte interfaces is still in its infancy. However, this also means that there is still room to develop new theoretical and numerical approaches. This makes this field challenging but at the same time rather exciting and rewarding.

There is one further challenge in the theoretical description of processes at solid/electrolyte interfaces related to the liquid nature of the electrolyte that has not been addressed so far. Many of the structural properties in thermodynamical equilibrium discussed so far are collectively known as mechanical properties [7] which can be routinely obtained from AIMD simulations [46, 47]. However, for the proper description of electrocatalytic reactions, the determination of reaction paths and barriers is important.

Here it is important to note that it is the free energy including the entropy that is the crucial quantity determining the effective barrier heights. This means that entropic effects have to be taken into account in order to evaluate the potential of mean force along the reaction path. Typically, free energy differences are obtained by performing constraint MD simulations using either umbrella sampling schemes [129, 130], free energy perturbation methods [131] or some other appropriate thermodynamic integration scheme. As these methods are compuationally rather time-consuming, there is also a need for the development of more efficient free energy sampling schemes [132].

VI. SOLID/ELECTROLYTE INTERFACES FOR NON-AQUEOUS ELECTROLYTES

So far we have almost entirely focused on aqueous electrolytes in our theoretical description of solid/electrolyte interfaces. This section which can be found in [1], describes solid/electrolyte interfaces with ionic liquids and organic solvents as electrolyte [135, 139].

VII. CONCLUSIONS

In this book chapter, we have tried describe the current status of the theory of solid/electrolyte interfaces. These systems are not only interesting from a fundamental point of view, but they are also of a high technological relevance, for example in electrochemical energy storage and conversion devices that are crucial for our future energy technology. Still, the theoretical description of solid/electrolyte interfaces faces many challenges. The liquid nature of the electrolyte requires a proper averaging over the many configurations compatible with the macroscopic variables defining the system. The computationally least demanding approach is first to average and then to perform the calculations which leads to a macroscopic description.

Many of the concepts still used today to discuss properties of solid/electrolyte interfaces have been developed more than one century ago using such a continuum approach. They form the basis of our current understanding. While they give qualitative guidelines, these macroscopic concepts alone are not sufficient for a quantitative description. For that purpose, an atomistic modeling is needed which, however, has to be combined with a proper thermodynamic treatment in the spirit of statistical mechanics.

This atomistic approach then requires the sampling over many possible contributions which represents a considerable computational challenge. Therefore inexpensive methods to describe the interatomic and intermolecular interactions are desirable. However, classical force fields typically do not describe both the interaction within the electrolyte as well as the electrode-electrolyte interaction equally reliably. More advanced interpolation schemes, on the other hand, often require a considerable training effort to obtain a proper parameter set.

Hence a quantum chemical approach from first principles is needed for a accurate treatment of the interatomic interactions. Here electronic structure calculations based on density functional theory are the method of choice as they combine numerical efficiency with an acceptable accuracy and reliability. Still, their numerical effort is large enough so that thermal averages over electrolyte configurations are not routinely done. Hence the influence of the electrolyte is often effectively into account either as thermodynamic reservoir or within implicit solvent models. The validity of these reasonable models can not be completely assessed as there is still hardly any realistic first-principles reference calculation for solid/electrolyte interfaces. The presence of varying electrode potentials for electrochemical solid/electrolyte interfaces adds further complexity to the theoretical treatment. Several different theoretical

approaches to represent external fields and varying electrode potentials exist, and all have their advantages and disadvantages. Thus there is still room for improvements in the realistic theoretical description of electrochemical solid-liquid interfaces. It is certainly fair to say that the first-principles treatment of these systems has not matured yet.

Nevertheless, there has been significant progress in the theoretical description of solid/electrolyte interfaces, at least as far as the conceptual and qualitative point of view is concerned. The still incomplete status of our knowledge about the microscopic nature of structures and processes at the electrochemical solid/liquid interface on a quantitative level makes this this research field demanding, but also exciting and rewarding.

---

[1] A. Groß, Theory of solid/electrolyte interfaces, in *Surface and Interface Science, Vol. 7: Solid/Liquid and Biological Interfaces*, edited by K. Wandelt, Wiley-VCH, Weinheim, 2015.

[2] R. Schlögl, ChemSusChem **3** (2010) 209.

[3] D. M. Kolb, Surf. Sci. **500** (2002) 722.

[4] A. Groß and S. Schnur, Computational chemistry applied to reactions in electrocatalysis, in *Catalysis in Electrochemistry: From Fundamentals to Strategies for Fuel Cell Development*, edited by E. Santos and W. Schmickler, pages 165–196, Wiley, 2011.

[5] A. Michaelides, Appl. Phys. A **85** (2006) 415.

[6] K. Reuter and M. Scheffler, Phys. Rev. B **65** (2001) 035406.

[7] A. R. Leach, *Molecular Modelling: Principles and Applications*, Pearson, Harlow, 2nd edition, 2001.

[8] J. K. Nørskov, J. Rossmeisl, A. Logadottir, L. Lindqvist, J. R. Kitchin, T. Bligaard, and H. Jónsson, J. Phys. Chem. B **108** (2004) 17886.

[9] J. K. Nørskov, T. Bligaard, A. Logadottir, J. R. Kitchin, J. G. Chen, S. Pandelov, and U. Stimming, J. Electrochem. Soc. **152** (2005) J23.

[10] W. Schmickler and E. Santos, *Interfacial Electrochemistry*, Springer, Berlin, 2nd edition, 2010.

[11] H. A. Hansen, I. C. Man, F. Studt, F. Abild-Pedersen, T. Bligaard, and J. Rossmeisl, Phys. Chem. Chem. Phys. **12** (2010) 283.

[12] J. A. Keith, G. Jerkiewicz, and T. Jacob, ChemPhysChem **11** (2010) 2779.

[13] T. Roman and A. Groß, Phys. Rev. Lett. **110** (2013) 156804.

[14] F. Gossenberger, T. Roman, and A. Groß, Surf. Sci. (2014) doi: 10.1016/j.susc.2014.01.021.

[15] J. Inukai, Y. Osawa, and K. Itaya, J. Phys. Chem. B **102** (1998) 10034.

[16] B. Obliers, P. Broekmann, and K. Wandelt, J. Electroanal. Chem. **554-555** (2003) 183 .

[17] J. Greeley, I. E. L. Stephens, A. S. Bondarenko, T. P. Johansson, H. A. Hansen, T. F.

Jaramillo, J. Rossmeisl, I. Chorkendorff, and J. K. Nørskov, Nat. Chem. **1** (2009) 552.
[18] I. E. L. Stephens, A. S. Bondarenko, U. Gronbjerg, J. Rossmeisl, and I. Chorkendorff, Energy Environ. Sci. **5** (2012) 6744.
[19] V. Viswanathan, H. A. Hansen, J. Rossmeisl, and J. K. Nrskov, ACS Catalysis **2** (2012) 1654.
[20] H. A. Gasteiger, S. S. Kocha, B. Sompalli, and F. T. Wagner, Appl. Catal. B **56** (2005) 9 .
[21] H. Helmholtz, Pogg. Ann. **89** (1853) 211.
[22] L. G. Gouy, J. Phys. **9** (1910) 457.
[23] D. L. Chapman, Phil.Mag. **25** (1913) 475.
[24] O. Stern, Z. Electrochem. **30** (1924) 508.
[25] A. Klamt, J. Phys. Chem. **99** (1995) 2224.
[26] K. Mathew, R. Sundararaman, K. Letchworth-Weaver, T. A. Arias, and R. G. Hennig, J. Chem. Phys. **140** (2014) 084106.
[27] J. I. Siepmann and M. Sprik, J. Chem. Phys. **102** (1995) 511.
[28] P. S. Crozier, R. L. Rowley, and D. Henderson, J. Chem. Phys. **113** (2000) 9202.
[29] R. Bukowski, K. Szalewicz, G. C. Groenenboom, and A. van der Avoird, Science **315** (2007) 1249.
[30] E. Spohr, J. Phys. Chem. **93** (1989) 6171.
[31] E. Spohr, J. Chem. Phys. **107** (1997) 6342.
[32] K. Raghavan, K. Foster, K. Motakabbir, and M. Berkowitz, J. Chem. Phys. **94** (1991) 2110.
[33] X. Xia and M. L. Berkowitz, Phys. Rev. Lett. **74** (1995) 3193.
[34] M. S. Daw and M. I. Baskes, Phys. Rev. B **29** (1984) 6443.
[35] M. S. Daw, S. M. Foiles, and M. I. Baskes, Mater. Sci. Rep. **9** (1993) 252.
[36] W. A. Goddard III., B. V. Merinov, A. C. T. van Duin, T. Jacob, M. Blanco, V. Molinero, S. S. Jang, and Y. H. Jang, Molecular Simulation **32** (2003) 251.
[37] S. Lorenz, M. Scheffler, and A. Groß, Phys. Rev. B **73** (2006) 115431.
[38] T. Morawietz and J. Behler, J. Phys. Chem. A **117** (2013) 7356.
[39] A. Warshel and R. M. Weiss, J. Am. Chem. Soc. **102** (1980) 6218.
[40] H. Lin and D. G. Truhlar, Theor. Chem. Acc. **117** (2007) 185.
[41] F. Wilhelm, W. Schmickler, R. R. Nazmutdinov, and E. Spohr, J. Phys. Chem. C **112** (2008) 10814.
[42] F. Wilhelm, W. Schmickler, R. R. Nazmutdinov, and E. Spohr, Electrochim Acta **56** (2011) 10632.
[43] W. Schmickler, F. Wilhelm, and E. Spohr, Electrochim. Acta **101** (2013) 341.
[44] A. Groß, Surf. Sci. **500** (2002) 347.
[45] J. Hafner, C. Wolverton, and G. Ceder, MRS Bulletin **31** (2006) 659.
[46] S. Schnur and A. Groß, New J. Phys. **11** (2009) 125003.
[47] D. Marx and J. Hutter, *Ab initio Molecular Dynamics: Basic Theory and Advanced Methods*, Cambridge University Press, Cambridge, 2009.

[48] A. K. Soper, J. Phys.: Condens. Matter **19** (2007) 335206.
[49] K. Forster-Tonigold and A. Groß, J. Chem. Phys. **141** (2014) 064501.
[50] B. Santra, A. Michaelides, M. Fuchs, A. Tkatchenko, C. Filippi, and M. Scheffler, J. Chem. Phys. **129** (2008) 194111.
[51] J. P. Perdew, K. Burke, and M. Ernzerhof, Phys. Rev. Lett. **77** (1996) 3865.
[52] B. Hammer, L. B. Hansen, and J. K. Nørskov, Phys. Rev. B **59** (1999) 7413.
[53] H. Do and N. A. Besley, J. Chem. Phys. **137** (2012) 134106.
[54] J. Paier, M. Marsman, and G. Kresse, J. Chem. Phys. **127** (2007) 024103.
[55] M. V. Fernández-Serra and E. Artacho, J. Chem. Phys. **121** (2004) 11136.
[56] J. VandeVondele, F. Mohamed, M. Krack, J. Hutter, M. Sprik, and M. Parrinello, J. Chem. Phys. **122** (2005) 014515.
[57] L.-M. Liu, M. Krack, and A. Michaelides, J. Chem. Phys. **130** (2009) 234702.
[58] S. Grimme, J. Comput. Chem. **25** (2004) 1463.
[59] S. Grimme, J. Antony, S. Ehrlich, and H. Krieg, J. Chem. Phys. **132** (2010) 154104.
[60] A. Tkatchenko and M. Scheffler, Phys. Rev. Lett. **102** (2009) 073005.
[61] A. Møgelhøj, A. K. Kelkkanen, K. T. Wikfeldt, J. Schiøtz, J. J. Mortensen, L. G. M. Pettersson, B. I. Lundqvist, K. W. Jacobsen, A. Nilsson, and J. K. Nørskov, J. Phys. Chem. B **115** (2011) 14149.
[62] J. Carrasco, B. Santra, J. Klimeč, and A. Michaelides, Phys. Rev. Lett. **106** (2011) 026101.
[63] K. Tonigold and A. Groß, J. Comput. Chem. **33** (2012) 695.
[64] C. Zhang, J. Wu, G. Galli, and F. Gygi, J. Chem. Theory Comput. **7** (2011) 3054.
[65] I.-C. Lin, A. P. Seitsonen, I. Tavernelli, and U. Rothlisberger, J. Chem. Theory Comput. **8** (2012) 3902.
[66] G. C. Lie and E. Clementi, Phys. Rev. A **33** (1986) 2679.
[67] J. A. Morrone and R. Car, Phys. Rev. Lett. **101** (2008) 017801.
[68] B. Chen, I. Ivanov, M. L. Klein, and M. Parrinello, Phys. Rev. Lett. **91** (2003) 215503.
[69] S. Fritsch, R. Potestio, D. Donadio, and K. Kremer, J. Chem. Theory Comput. **10** (2014) 816.
[70] D. Marx, ChemPhysChem **7** (2006) 1848.
[71] A. Groß and M. Scheffler, J. Vac. Sci. Technol. A **15** (1997) 1624.
[72] A. Groß, C. M. Wei, and M. Scheffler, Surf. Sci. **416** (1998) L1095.
[73] P. A. Thiel and T. E. Madey, Surf. Sci. Rep. **7** (1987) 211.
[74] P. J. Feibelman, Science **295** (2002) 99.
[75] A. Roudgar and A. Groß, Surf. Sci. **597** (2005) 42.
[76] A. Roudgar and A. Groß, Chem. Phys. Lett. **409** (2005) 157.
[77] Y. Gohda, S. Schnur, and A. Groß, Faraday Discuss. **140** (2008) 233.
[78] A. Michaelides, V. A. Ranea, P. L. de Andres, and D. A. King, Phys. Rev. Lett. **90** (2003) 216102.
[79] S. Izvekov, A. Mazzolo, K. Van Opdorp, and G. A. Voth, J. Chem. Phys. **114** (2001) 3284.

[80] S. Izvekov and G. A. Voth, J. Chem. Phys. **115** (2001) 7196.
[81] S. Schnur and A. Groß, Catal. Today **165** (2011) 129.
[82] J. S. Filhol and M.-L. Bocquet, Chem. Phys. Lett. **438** (2007) 203.
[83] J. M. Heras and L. Viscido, Appl. Surf. Sci. **4** (1980) 238.
[84] E. Langenbach, A. Spitzer, and H. Lüth, Surf. Sci. **147** (1984) 179.
[85] M. Kiskinova, G. Pirug, and H. Bonzel, Surf. Sci. **150** (1985) 319.
[86] W. Hoffmann and C. Benndorf, Surf. Sc. **377-379** (1997) 681.
[87] Y. Lilach, L. Romm, T. Livneh, and M. Asscher, J. Phys. Chem. B **105** (2001) 2736.
[88] X. Lin and A. Groß, Surf. Sci. **606** (2012) 886.
[89] H. Ibach, Surf. Sci. **604** (2010) 377.
[90] H. Ibach, Surf. Sci. **606** (2012) 1534.
[91] A. Groß, F. Gossenberger, X. Lin, M. Naderian, S. Sakong, and T. Roman, J. Electrochem. Soc. **161** (2014) E3015 .
[92] T. Roman and A. Groß, Catal. Today **202** (2013) 183.
[93] T. J. Schmidt, P. N. Ross Jr., and N. M. Markovic, J. Electroanal. Chem. **524** (2002) 252 .
[94] N. M. Marković and P. N. Ross Jr., Surf. Sci. Rep. **45** (2002) 117.
[95] W. Schmickler, Chem. Rev. **96** (1996) 3177.
[96] R. Guidelli and W. Schmickler, Electrochim. Acta **45** (2000) 2317.
[97] O. M. Magnussen, Chem. Rev. **107** (2002) 679.
[98] D. V. Tripkovic, D. Strmcnik, D. van der Vliet, V. Stamenkovic, and N. M. Markovic, Faraday Discuss. **140** (2009) 25.
[99] P. Broekmann, M. Wilms, M. Kruft, C. Stuhlmann, and K. Wandelt, J. Electroanal. Chem. **467** (1999) 307.
[100] Y. Gründer, A. Drünkler, F. Golks, G. Wijts, J. Stettner, J. Zegenhagen, and O. M. Magnussen, Surf. Sci. **605** (2011) 1732.
[101] A. Groß, Surf. Sci. **608** (2013) 249 .
[102] A. Y. Lozovoi, A. Alavi, J. Kohanoff, and R. M. Lynden-Bell, J. Chem. Phys. **115** (2001) 1661.
[103] N. D. Mermin, Phys. Rev. **137** (1965) A 1441.
[104] C. D. Taylor, S. A. Wasileski, J.-S. Filhol, and M. Neurock, Phys. Rev. B **73** (2006) 165402.
[105] A. Alavi, J. Kohanoff, M. Parrinello, and D. Frenkel, Phys. Rev. Lett. **73** (1994) 2599.
[106] S. A. Wasileski and M. J. Janik, Phys. Chem. Chem. Phys. **10** (2008) 3613.
[107] J. S. Filhol and M. Neurock, Angew. Chem. Int. Ed. **45** (2006) 402.
[108] C. L. Fu and K. M. Ho, Phys. Rev. Lett. **63** (1989) 1617.
[109] K. P. Bohnen and D. M. Kolb, Surf. Sci. **407** (1998) L629.
[110] A. Y. Lozovoi and A. Alavi, Phys. Rev. B **68** (2003) 245416.
[111] J. G. Che and C. T. Chan, Phys. Rev. B **67** (2003) 125411.
[112] J. Zhao, C. T. Chan, and J. G. Che, Phys. Rev. B **75** (2007) 085435.
[113] S. Trasatti, Surf. Sci. **335** (1995) 1.

[114] E. Skúlason, G. S. Karlberg, J. Rossmeisl, T. Bligaard, J. Greeley, H. Jónsson, and J. K. Nørskov, Phys. Chem. Chem. Phys. **9** (2007) 3241.
[115] S. Trasatti, Pure Appl. Chem. **58** (1986) 955.
[116] A. Logadottir, T. H. Rod, J. K. Nørskov, B. Hammer, S. Dahl, and C. J. H. Jacobsen, J. Catal. **197** (2001) 229.
[117] J. Cheng and P. Hu, J. Am. Chem. Soc. **130** (2008) 10868.
[118] M. Otani and O. Sugino, Phys. Rev. B **73** (2006) 115407.
[119] O. Sugino, I. Hamada, M. Otani, Y. Morikawa, T. Ikeshoji, and Y. Okamoto, Surf. Sci. **601** (2007) 5237.
[120] M. Otani, I. Hamada, O. Sugino, Y. Morikawa, Y. Okamoto, and T. Ikeshoji, Phys. Chem. Chem. Phys. **10** (2008) 3609.
[121] I. Hamada, O. Sugino, N. Bonnet, and M. Otani, Phys. Rev. B **88** (2013) 155427.
[122] Y. Qian, I. Hamada, M. Otani, and T. Ikeshoji, Catal. Today **202** (2013) 163.
[123] J. Rossmeisl, E. Skúlason, M. J. Björketun, V. Tripkovic, and J. K. Nørskov, Chem. Phys. Lett. **466** (2008) 68.
[124] N. M. Marković, B. N. Grgur, and P. N. Ross, J. Phys. Chem. B **101** (1997) 5405.
[125] J. Greeley, J. K. Nørskov, L. A. Kibler, A. M. El-Aziz, and D. M. Kolb, Chem. Phys. Chem. **7** (2006) 1032.
[126] N. Bonnet, T. Morishita, O. Sugino, and M. Otani, Phys. Rev. Lett. **109** (2012) 266101.
[127] W. B. Schneider and A. A. Auer, Beilstein J. Nanotechnol. **5** (2014) 668.
[128] S. Nosé, J. Chem. Phys. **81** (1984) 511.
[129] G. M. Torrie and J. P. Valleau, J. Comp. Phys. **23** (1977) 187 .
[130] C. Hartnig and M. T. M. Koper, J. Chem. Phys. **115** (2001) 8540.
[131] R. W. Zwanzig, J. Chem. Phys. **22** (1954) 1420.
[132] C. D. Christ and W. F. van Gunsteren, J. Chem. Phys. **126** (2007) 184110.
[133] P. Wasserscheid and W. Keim, Angew. Chem. Int. Ed. **39** (2000) 3772.
[134] M. Armand, F. Endres, D. R. MacFarlane, H. Ohno, and B. Scrosati, Nature Mater. **8** (2009) 621.
[135] F. Buchner, K. Forster-Tonigold, B. Uhl, D. Alwast, N. Wagner, H. Farkhondeh, A. Groß, and R. J. Behm, ACS Nano **7** (2013) 7773.
[136] D. Künzel, K. Tonigold, J. Kučera, M. Roos, H. E. Hoster, R. J. Behm, and A. Groß, ChemPhysChem **12** (2011) 2242.
[137] C. Meier, K. Landfester, D. Künzel, T. Markert, A. Groß, and U. Ziener, Angew. Chem. Int. Ed. **47** (2008) 3821.
[138] C. Meier, M. Roos, D. Künzel, A. Breitruck, H. E. Hoster, K. Landfester, A. Gross, R. J. Behm, and U. Ziener, J. Phys. Chem. C **114** (2010) 1268.
[139] D. Künzel and A. Groß, Beilstein J. Nanotechnol. **4** (2013) 269277.
[140] D. Künzel, T. Markert, A. Groß, and D. M. Benoit, Phys. Chem. Chem. Phys. **11** (2009)

8867.